Drive laser system for the DC-SRF photoinjector at Peking University *

Zhi-Wen Wang(王志文)   Sen-Lin Huang(黄森林)[1)]   Lin Lin(林林)   Gang Zhao(赵刚)

Sheng-Wen Quan(全胜文)   Ke-Xin Liu(刘克新)   Jia-Er Chen(陈佳洱)

State Key Laboratory of Nuclear Physics and Technology, Institute of Heavy Ion Physics, Peking University, Beijing 100871, China

Abstract: Photoinjectors are widely used for linear accelerators as electron sources to generate high-brightness electron beams. The drive laser, which determines the timing structure and quality of the electron beam, is a crucial component of a photoinjector. A new drive laser system has been designed and constructed for the upgraded 3.5-cell DC-SRF photoinjector at Peking University. The drive laser system consists of a 1064 nm laser oscillator, a four-stage amplifier, second and fourth harmonic generators, an optical system to transfer the UV pulses to the photocathode, and a synchronization system. The drive laser system has been successfully applied during stable operation of the DC-SRF photoinjector and its performance meets requirements. A 266 nm laser with an average power close to 1 W can be delivered to illuminate the Cs_2Te photocathode and the instability is less than 5% for long time operation. The design considerations for improving the UV laser quality, a detailed description of the laser system, and its performance are presented in this paper.

Keywords: drive laser, amplifier, harmonic generation, photoinjector

PACS: 07.77.Ka, 42.55.-f, 42.62.-b   **DOI:** 10.1088/1674-1137/40/1/017004

1 Introduction

Photoinjectors have been developed for over two decades, and are widely used now for linear accelerators as electron sources to generate high-brightness electron beams. Except for determining the basic properties of the electron bunches, such as their time sequence, duration, and the amount of bunch charge, the driver laser of a photoinjector also affects the stability of the produced bunch and its synchronization accuracy to the accelerator RF field, as well as the emittance of the electron beam. As a crucial component of a photoinjector, drive laser systems are generally developed by laboratories themselves because there are few commercially available products which can meet the requirements of different applications. For example, for the ERL-FEL at JLab, a drive laser with pulse repetition rate of 75 MHz, wavelength of 532 nm, and average power of 25 W was developed [1]. For the FLASH at DESY Hamburg, a drive laser with pulse repetition rate of 1 MHz or 3 MHz, wavelength of 262 nm, and pulse energy of 30 μJ was developed [2].

The DC-SRF photoinjector, which combines a DC pierce gun and a superconducting radio frequency (SRF) cavity, was first proposed by Peking University in 2001 [3]. It is a potential SRF photoinjector candidate to provide an electron beam with medium average current,

low emittance, and short bunch length. A prototype of this kind of injector with a 1.5-cell SRF cavity was designed and constructed in 2004 [4]. Preliminary experiments at 4 K demonstrated the feasibility of DC-SRF structure. An upgraded DC-SRF photoinjector with a 3.5-cell large-grain SRF cavity has been designed and constructed recently and beam experiments carried out. The results indicated that the drive laser system used for the 1.5-cell prototype [5] is not stable enough to obtain a high-quality electron beam. The main problems are low laser power at 1064 nm and instability of second harmonic generation (SHG) and fourth harmonic generation (FHG) induced by thermal effects. We have therefore designed and constructed a new drive laser system, which is composed of a 1064 nm laser oscillator, a four-stage amplifier, harmonic generation system, laser beam transport optics, etc, to meet the requirements of the 3.5-cell DC-SRF photoinjector. In this paper, we introduce this new drive laser system and discuss its special features in detail.

2 Basic parameters and layout of the drive laser system

The main parameters of the DC-SRF photoinjector are shown in Table 1. Considering the stability and the less stringent vacuum environment requirements, a

Cs_2Te photocathode is used even though it does not have a very high quantum efficiency and needs to be driven by ultraviolet (UV) laser with a wavelength around 260 – 270 nm.

Table 1.   Main parameters of the DC-SRF photoinjector.

parameter	value	unit
RF frequency	1300	MHz
bunch charge	>12	pC
average current	>1	mA
normalized emittance	~1.2	μm
bunch length (FWHM)	~3	ps
beam energy	$3-5$	MeV

The primary parameters of the drive laser can be derived from the requirements of the DC-SRF photoinjector. The average current and bunch charge shown in Table 1 indicate that the drive laser does not need to have a repetition rate as high as 1.3 GHz. We have chosen a repetition rate of 81.25 MHz, the 16th harmonic of the RF frequency of the 3.5-cell SRF cavity. Since most commercially available laser oscillators work in the infrared (IR) wavelength region, a laser oscillator with a wavelength of 1064 nm, which was used for the 1.5-cell DC-SRF photoinjector prototype, is still adopted for the new drive laser system. Nonlinear crystals will be used to convert the IR pulses to UV pulses with a wavelength of 266 nm.

The output power is another important parameter of the drive laser system. The photocurrent can be described with the formula [6]

$$I[\text{mA}] = \frac{\lambda[\text{nm}]}{124} \times P_{\text{laser}}[\text{W}] \times Q.E.[\%], \tag{1}$$

where λ is the wavelength of the drive laser and $Q.E.$ is the quantum efficiency of the photocathode. The $Q.E.$ of the Cs_2Te photocathode has a maximum of around 10%, but it is very sensitive to the vacuum environment. Considering a safety margin of 10, a UV laser with average power of at least 0.5 W is needed to obtain an average electron beam current of more than 1 mA. The expected electron bunch length from the DC-SRF photoinjector is around 3 ps (FWHM). According to the simulation of bunch compression by the RF field in the 3.5-cell SRF cavity [7], the drive laser is required to have a pulse length of less than 6 ps (FWHM).

An optical layout of the drive laser system is shown in Fig. 1 and a photo of the laser system can be seen in Fig. 2. The system consists of a 1064 nm laser oscillator, a four-stage amplifier, a harmonic generation system, an optical system to transfer the UV pulses to the photocathode, and a synchronization system. The laser oscillator produces seed pulses with a repetition rate of 81.25 MHz. These pulses are synchronized to the RF field in the linac cavities with sub-picosecond timing jitter. The 1064 nm seed laser pulse from the oscillator is amplified by about 9 times in power and then converted to 532 nm green laser and 266 nm UV laser by the harmonic generators. The UV pulses are finally transported to the cathode of the DC-SRF photoinjector through suitable imaging optics. The details of the design considerations and the performance of the laser system will be described in the following sections.
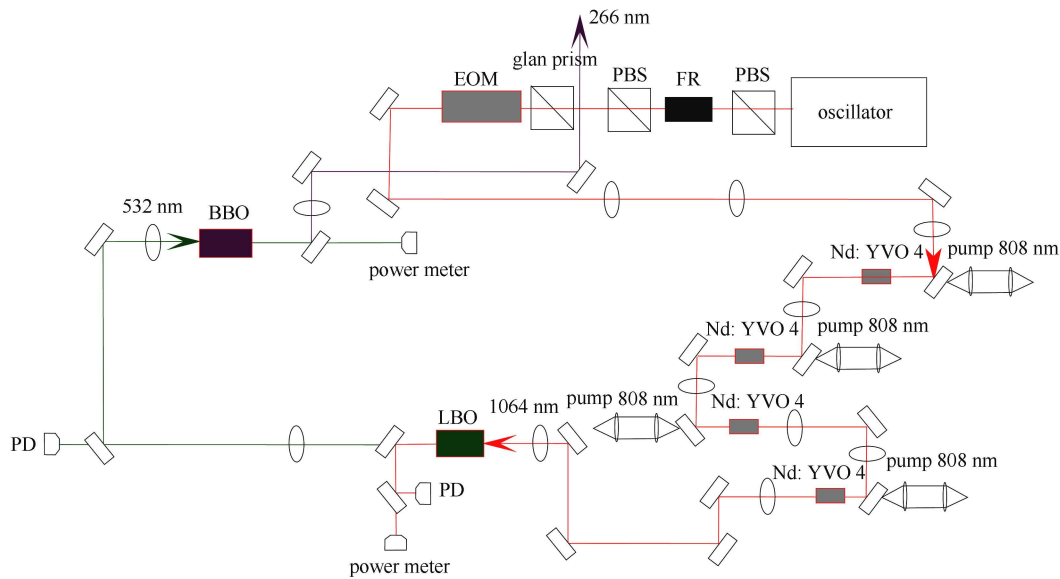

Fig. 1.   (color online) Schematic layout of the drive laser system for the DC-SRF photoinjector.
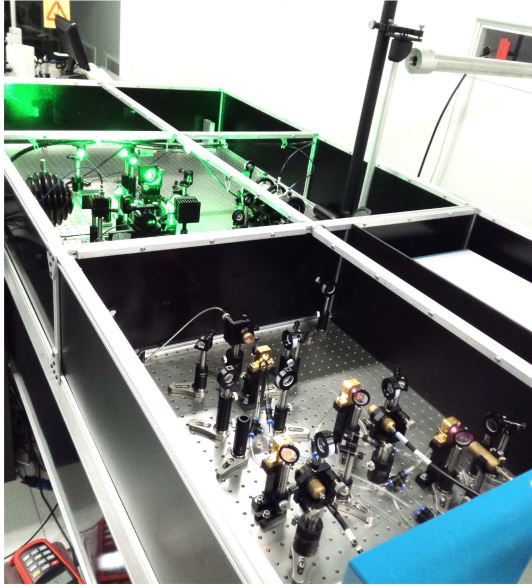
Fig. 2.   (color online) A photo of the drive laser system for the DC-SRF photoinjector. The laser system is shielded in a box made of 3-mm thick aluminum plate.

3   Laser oscillator and amplifier

The 1064 nm laser is configured as a master oscillator power amplifier (MOPA). The master oscillator, Time-Bandwidth Products GE-100-XHP series, is a passively mode-locked, diode-pumped solid-state laser. The laser pulse from the oscillator has a repetition rate of 81.25 MHz and a nearly Gaussian temporal profile with an FWHM of 10 ps. The pulse-forming process is started and stabilized by a semiconductor saturable absorber mirror (SESAM), which also forms one end of the laser cavity. It is mounted on a translation stage driven by a picomotor, through which the cavity length can be adjusted. The cavity can also be fine-tuned using a piezo. A photodiode with nanosecond-level response is applied to monitor the laser pulses. Its signal is phase-locked to the accelerator RF using Time-Bandwidth CLX-1100 timing stabilizer.

To obtain more stable UV laser pulses, we prefer to use shorter nonlinear crystals for wavelength conversion. To compensate for the reduction of wavelength conversion efficiency, much higher 1064 nm laser power is needed. A 1064 nm laser amplifier should therefore be applied. Nd-doped laser materials are widely used for amplifiers in many laboratories, such as FLASH, Daresbury, PITZ, FZD Rossendorf, Fermilab, SLAC, etc., due to their high efficiency, good reliability, relatively simple setup, and low maintenance costs. Moreover, low doping concentration Nd:YVO4 crystal has an advantage in reducing thermal loading density and achieving more uniform absorption under high intensity pumping. As a

result, a-cut 0.3% Nd-ion concentration bulk Nd:YVO4 crystals (3 mm × 3 mm × 10 mm) are used for the amplifier. Both end faces of the Nd:YVO4 crystals are dichroic coated for high transmittance at 1064 nm and 808 nm. The crystals are wrapped with indium foil and placed in copper heat sinks with water cooling.

For high power output and good beam quality, the amplifier is configured as four single-pass, single-end-pumped stages. Because of the high repetition rate of the laser pulses, CW laser diode modules need to be used as the pump source to keep the laser power instability below 1%. Four sets of LIMO 808 nm off-board laser diode modules, with output power of 37 W, are therefore chosen as the pump sources. The pump lasers, transported through 400 μm fibers, are coupled onto the end face of the Nd:YVO4 crystals using imaging optics. The pump source couplers are placed in holders which can realize four-dimensional translation and tilt adjustment. This is convenient for optimization and maintenance of the amplifier.

To direct the 1064 nm laser through the Nd:YVO4 crystals, four dichroic mirrors, anti-reflection (AR) coated at 808 nm and high-reflection (HR) coated at 1064 nm, are placed between the pump source couplers and crystals with an incident angle of 45° (see Fig. 1). Telescope optics are used both to match the 1064 nm laser beam into the Nd:YVO4 crystals and to expand the laser beam when necessary to avoid damage to the optical elements due to too high a laser power density. To prevent the amplified laser beam from reflecting back into the master oscillator, the amplifier is isolated from the oscillator using a Faraday rotator.
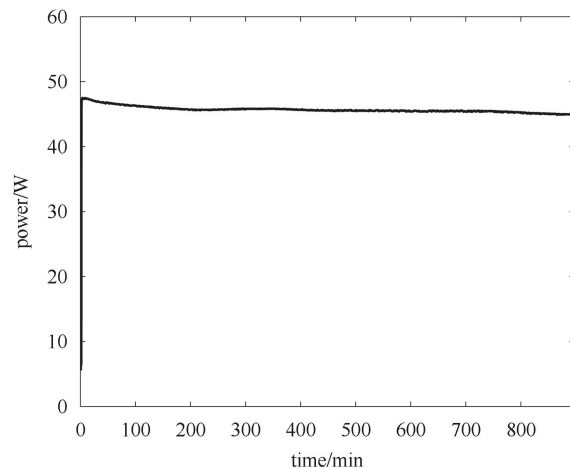

Fig. 3.   1064 nm laser power after the four-stage amplifier, during long-term monitoring.

The 1064 nm laser power is 5 W before the first stage of the amplifier. In CW operation, at a pump current of 45 A, 45 W stable output has been obtained from the MOPA system (see Fig. 3). The net power gain of the

amplifier is 40 W. Compared to the total pump power of the four laser diode modules (148 W), the total optical–optical efficiency is about 27%. Figure 4 shows the average laser power after the amplifier versus the current of the pump diode power supplies. It can be seen from the figure that the average laser power grows rapidly as the current increases above 25 A. The increase of the laser power slows down around 42–45 A. The operation pump current is therefore set at 45 A, which is still within the safe region.
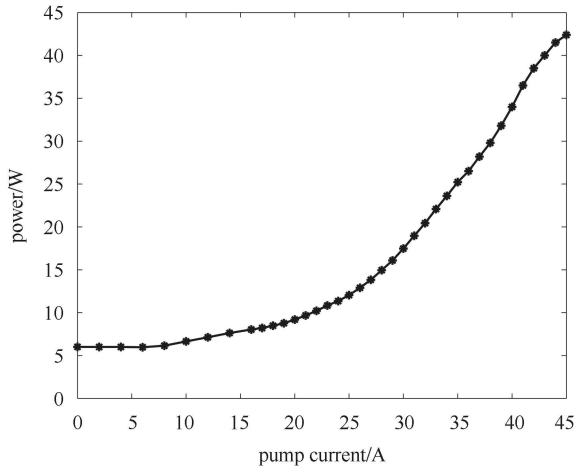

Fig. 4.   Amplified 1064 nm laser power as a function of the amplifier pump diode current.

4   Harmonic generation system

To obtain the UV laser pulses required by the Cs_2Te cathode in the DC-SRF photoinjector, a two-stage cascaded harmonic generation system has been designed. As the first stage, an LBO crystal is used for SHG. The 532 nm laser from LBO then traverses a BBO crystal for FHG. The LBO and BBO crystals are chosen for SHG and FHG because they are non-critically phase-matched and have high damage threshold and high conversion efficiency.

The LBO crystal has a length of 15 mm and a cross section of 4 mm × 4 mm and is cut at θ of 90° and φ of 10.6°. Its end faces are AR coated for high transmittance ($T > 99.8\%$) at 1064 nm. The crystal is mounted in a thermostat, whose temperature can be remotely adjusted for optimized phase-matching angle. During the operation, the temperature is controlled at (45 ± 0.1)°C.

For FHG using BBO crystal, the large walk-off angle [8] caused by BBO crystal's large birefringence limits the conversion efficiency and makes the transverse profile of UV laser beam far from Gaussian distribution. This problem can be solved by using a walk-off compensation system, where two or more crystals having the same cut and length [9–11] are arranged with the crystal optic axes in alternating directions (see Fig. 5). In our system, a

pair of 2-mm long BBO crystals, which have a 4 mm × 4 mm cross section and are cut at θ of 47.7° and φ of 0°, are used. The BBO crystal end faces are AR-coated for high transmittance at 532 nm ($T > 99.8\%$) and 266 nm ($T > 99.5\%$).
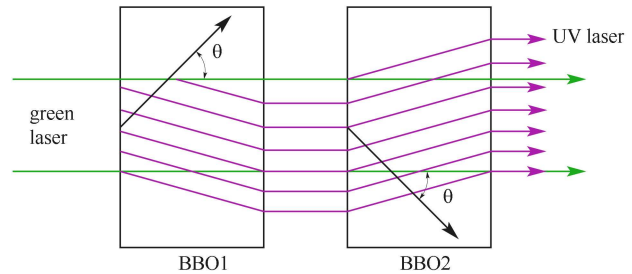

Fig. 5.   (color online) Walk-off compensation arrangement using two BBO crystals for second harmonic generation from green laser to UV laser. The extraordinary UV beam walk-off in the first crystal is compensated by propagation through the second crystal, where the extraordinary UV beam walks onto the two ordinary beams from the two crystals.

As shown in Fig. 1, demagnifying telescopes located before the LBO and BBO crystals are used to reduce the diameter of the beam to 10s μm for better wavelength conversion performance. After the LBO crystal, a set of lenses and a dichroic mirror is employed to collimate the SHG beam and eliminate the residual 1064 nm laser. After the BBO crystals, another set of lenses and dichroic mirror is also employed to collimate the FHG beam and eliminate the residual 532 nm laser.
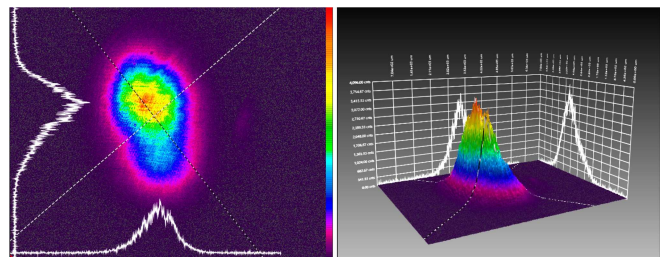

Fig. 6.   (color online) Two-dimensional and three-dimensional transverse profiles of the 266 nm UV laser.

The measured conversion efficiencies of the SHG, from 1064 nm to 532 nm, and FHG, from 532 nm to 266 nm, are 40% and 5.6%, respectively. The total conversion efficiency, from 1064 nm to 266 nm, is better than 2%. The 266 nm UV laser beam profile has been improved compared to our previous laser system using single-BBO (see Fig. 6). It can be further improved using transverse distribution shaping techniques. There is

still enough room for increasing the conversion efficiency by different design of the harmonic generation system. In particular, an electro-optic (EO) modulator is being used to adjust the repetition rate of the 1064 nm laser pulses. Using the EO modulator, the laser pulse repetition rate can be reduced as desired. This will benefit the harmonic generation system, since the laser pulse energy can be increased while the average power remains unchanged.

5   Stability improvement of the drive laser system

The laser system is installed in a class 1000 cleanroom, where the temperature is controlled at $(20\pm0.5)°C$ and humidity less than 30%. Because of the air conditioning system, air flow exists in this cleanroom. To reduce the vibration caused by air flow, the main parts of the drive laser system are covered in a shielding box made of 3 mm thick aluminum plate (see Fig. 2).
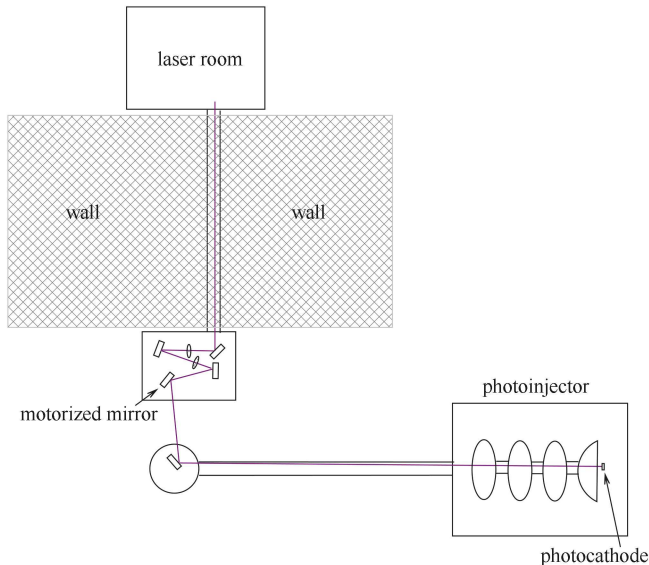

Fig. 7.   (color online) Optical beam line for 266 nm UV laser.

In the previous drive laser system, the FHG system was installed in our SRF accelerator hall and the instabilities of both laser power and laser beam pointing became enlarged. In our new design, the FHG has been moved into the cleanroom. This makes the 266 nm laser transport a longer distance (about 20 m) to the reflecting mirror installed in the vacuum chamber of the electron beam line (see Fig. 7), and it is more difficult to project the laser beam to the photocathode. A motorized mirror mount has been designed and installed in the optical beam line for precise remote control of a 45° mirror right before the in-vacuum reflecting mirror. The incident point of the UV laser on the surface of the photocathode

can therefore be precisely scanned using this motorized mirror mount. The optical beam line is shielded to prevent air turbulence caused by a temperature differential and air flow.

6   Performance of the drive laser

The performance of the drive laser system has been investigated, including the power instability, the beam pointing instability, and the synchronization with accelerator RF signal. The long-term instability of the 1064 nm and 266 nm lasers were monitored using a power meter integrated into our control system. Figure 3 and Fig. 8 present the results of our latest monitoring of the 1064 nm laser and the 266 nm laser, respectively. During the measurements, the drive laser system was operated with the 1064 nm laser power of 45 W and the 266 nm laser power close to 1 W. The long-term instability of the UV laser power is less than 5% after the warming up of the laser system. This is sufficient for the DC-SRF photoinjector beam experiments.
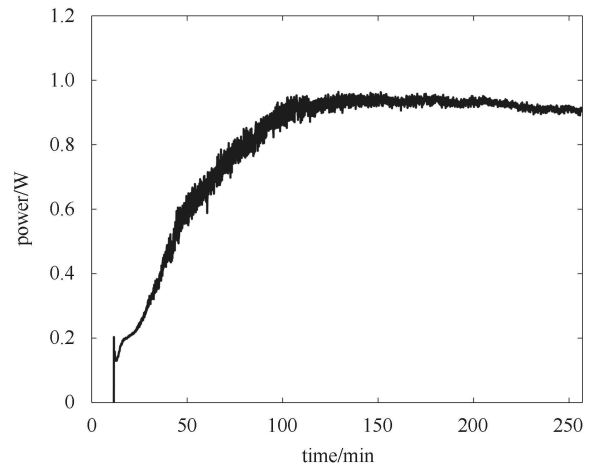

Fig. 8.   266 nm laser power from warming up to stable operation.

The pointing stability of the 266 nm laser beam was estimated by analyzing the laser beam on a virtual photocathode using a beam profiler. The pointing instability was measured to be 8 µrad rms in both horizontal and vertical direction. This is a remarkable improvement on our previous drive laser system.

A phase detector, integrated with a fast photodiode, was used to monitor the phase difference between the 1064 nm laser pulses and accelerator RF field. The timing jitter, derived from the phase difference, was less than 1 ps rms. The phase difference between the 266 nm laser pulses and accelerator RF field was measured by a UV phase detector, from which the timing jitter is derived to be less than 1 ps rms. This means that the UV laser beam is well isolated from environmental vibrations.

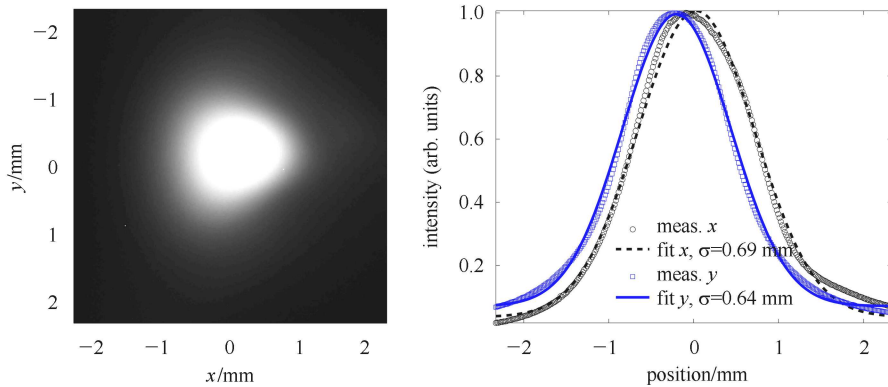The new drive laser system has been applied in the

Fig. 9.   (color online) The image (left) and transverse profile (right) of electron beam. The horizontal (x) and vertical (y) distributions are plotted as black circles and blue squares, respectively. The distributions are fitted to a Gaussian function and the results are plotted as the black dashed curve and blue solid curve.

beam test and stable operation of the DC-SRF photoinjector. With 0.5 W 266 nm laser power, a stable electron beam has been obtained with an energy of 3.4 MeV and a normalized emittance of 2 mm·mrad. The average beam current reached 1 mA and was kept at 0.55 mA for longterm operation. The electron beam current is not limited by the drive laser system at present.

A typical transverse profile for the electron beam during the operation of the DC-SRF photoinjector is shown in Fig. 9. One can see from the figure that the electron beam has a two-dimensional Gaussian distribution. The rms size of the measured electron beam is 0.69 mm in the horizontal direction and 0.64 mm in the vertical direction.

7   Conclusion

A new drive laser system has been successfully designed and constructed for the upgraded 3.5-cell DC-SRF photoinjector at Peking University. Double BBO crystals in the FHG are adopted to reduce the walk-off effect. Careful design makes the system more compact and isolated from interference from the surrounding environment. A 266 nm laser with average power close to 1 W can be delivered to illuminate the Cs_2Te photocathode and the instability is less than 5% for long-term operation. The pointing instability was measured to be 8 μ rad rms in both horizontal and vertical direction. The drive laser system has been applied in the DC-SRF photoinjector beam experiments and the performance meets the requirements. Recently, an EO modulator has been installed in our laser system. Using the EO modulator, the laser pulse repetition rate can be reduced as desired. This laser system, especially the harmonic generators, may be further developed to make the best use of this new capability.

References

1 S. Zhang, Drive Laser Systems for Electron Accelerators and Free-Electron-Lasers Based on Photocathode-Injector Energy-Recovery-Linac, in *Proceedings of ERL09* (Ithaca, New York, 2009), WG110
2 Ingo Will, Horst I. Templin, Siegfried Schreiber, and Wolfgang Sandner, Optics Express, **19**: 23770 (2011)
3 K. Zhao, J. K. Hao, Y. L. Hu et al, Nucl. Instrum. Methods A, **475**: 564 (2001)
4 J. K. Hao, X. Y. Lu, Y. T. Ding et al, Nucl. Instrum. Methods A, **557**: 138 (2006)
5 X. Y. Lu, L. Lin, K. Zhao, and S. W. Zhang, HEP & NP, **28**: 8 (2004) (in Chinese)

6 E. J. Montgomery, D. W. Feldman, Z. Pan et al, in *Proceedings of PAC07*, (Albuquerque, New Mexico, 2007), p.1206
7 F. Zhu, S.W. Quan, J.K. Hao et al, Status of the DC-SRF Photoinjector for PKU-SETF, in *Proceedings of SRF2011* (Chicago, IL, 2011), p.973
8 G. D. Boyd, D. A. Kleinman, J. Appl. Phys., **39**: 3597 (1968)
9 C. Droz, H. Kouta, and Y. Kuwano., Optical Review, **6**: 97 (1999)
10 J. Friebe, K. Moldenhauer, E. M. Rasel et al, Opt. Comm., **261**: 300 (2006)
11 T. Onda, M. Shinnosuke, and I. Shoji, A New Walk-Off Compensating BBO Device with Thinner-Plae-Stacked Structrue Fabricated by Room-Temperature Bonding, in *Proccedings Nonlinear Optics 2013* (Kohala Coast, Hawaii, 2013), p.NTu3B.1